EUROPEAN ORGANIZATION FOR NUCLEAR RESEARCH
European Laboratory for Particle Physics

Internal Note/
ALICE reference number
ALICE-INT-2004-029 version 1.0
Institute reference number
[-]
Date of last change
2004-11-15

A High Resolution Electromagnetic Calorimeter based on Lead-Tungstate Crystals

Authors:

ALICE PHOS-calorimeter Collaboration:
D. V. Alexandrov[a], S. F. Burachas[a], M. S. Ippolitov[a], V. A. Lebedev[a], V. I. Manko[a*], S. A. Nikulin[a], A. S. Nyanin[a], I. G. Sibiriak[a], A. A. Tsvetkov[a], A. A. Vasiliev[a], A. A. Vinogradov[a], M. Yu. Bogolyubsky[b], Yu. V. Kharlov[b], S. A. Konstantinov[b],V.S.Petrov[b], B. V. Polishchuk[b], S. A. Sadovsky[b], V. A. Senko[b], A. S. Soloviev[b], V. A. Victorov[b], A. S. Vodopianov[c], P. V. Nomokonov[c], V. F. Basmanov[d], D. V. Budnikov[d], R. I. Ilkaev[d], A. V. Kuryakin[d], S. T. Nazarenko[d], V. T. Punin[d], Yu. I. Vinogradov[d], H. Delagrange[e], Y. Schutz[e,k], G. C. Balbestre[e], J. Diaz[e], A. Klovning[f], O. Mæland[f], O. H. Odland[f], B. Pommersche[f], Z. Yin[f], B. Skaali[g], D. Wormald[g], J. A. Mares[h], K. Ploak[h], A. Deloff[i], T. Dobrowolski[i], K. Karpio[i], M. Kozlowski[i], K. Redlich[i], T. Siemiarczuk[i], G. Stefanek[i], L. Tykarski[i], G. Wilk[i], T. Sugitate[j], K. Shigaki[j], R. Kohara[j].

[a]Russian Research Centre Kurchatov Institute, Moscow, Russia
[b]Institute for High Energy Physics, Protvino, Russia
[c]JINR, Dubna, Russia
[d]RFNC VNIIEF, Sarov, Russia
[e]SUBATECH, Nantes, France
[f]Department of Physics, University of Bergen, Bergen, Norway
[g]Department of Physics, University of Oslo
[h]Institute of Physics, Academy of Sciences of the Czech Republic, Prague, Czech Republic
[i]Soltan Institute for Nuclear Studies, Warsaw, Poland
[j]Hiroshima University, Kagamiyama, Higashi-Hiroshima, Japan
[k]CERN, Geneva, Switzerland

[†]This work was supported by:
Ministry of Atomic Energy and Ministry of Industry, Science and Technologies of Russian Federation;
INTAS, Contract No. 99-692;
Polish State Committee for Scientific Research, Grant No. 2P03B05724;
Grant-in-Aid No. 15340079, MEXT, Japan;
The Norwegian Research Council;

* Corresponding author. Tel.: +7-095-196-9101, +41-22-767-4747; fax: +41-22-767-9480.
E-mail addresses: Vladislav.Manko@cern.ch, manko@vskur4.mbslab.kiae.ru

Abstract:

A large-scale prototype of the PHOS electromagnetic spectrometer, which is part of the ALICE detector, has been built and tested. This prototype has 256 detector channels and is operated at -25$_{o}$C. Each detector channel is a lead tungstate crystal coupled to an Avalanche Photo-Diode with a low-noise preamplifier. The prototype includes a 16×16 crystal matrix, photo-detectors, analog and digital electronics, a thermo-stabilized cooling system, a light-emitting diode monitoring system, and a charged-particle detector acting as veto counter.
Results of measurements using electron and hadron beams of the CERN PS and SPS accelerators are discussed, and the performance of the prototype is evaluated.

Abstract

A large-scale prototype of the PHOS electromagnetic spectrometer, which is part of the ALICE detector, has been built and tested. This prototype has 256 detector channels and is operated at -25°C. Each detector channel is a lead tungstate crystal coupled to an Avalanche Photo-Diode with a low-noise preamplifier. The prototype includes a 16×16 crystal matrix, photo-detectors, analog and digital electronics, a thermo-stabilized cooling system, a light-emitting diode monitoring system, and a charged-particle detector acting as veto counter. Results of measurements using electron and hadron beams of the CERN PS and SPS accelerators are discussed, and the performance of the prototype is evaluated.

1 Introduction

ALICE (A Large Ion Collider Experiment) [1] is the dedicated heavy-ion experiment at the future Large Hadron Collider (LHC) at CERN. Detection and identifying energetic photons emitted in collisions of heavy nuclei at ultrarelativistic energies is one of the experimental tasks of ALICE. The ALICE experiment includes, for that purpose, an electromagnetic spectrometer, the PHOS (PHOton Spectrometer).

Central Pb-Pb collisions at LHC energies will generate very high particle densities. Upper estimates are as high as 8000 charged particles per unit of rapidity, at mid-rapidity. Such high particle densities require, for photon detection and identification, the use of a highly segmented calorimeter with individual detection cells of small cross-section made out of a very dense material having the smallest possible Molière radius.

The PHOS has been designed to cover the pseudorapidity from -0.12 to +0.12 and an azimutal domain of 100 degrees. The detector is built as 5 identical modules, each with 3584 detection channels and 17920 in total. Each detection channel consists of a lead-tungstate crystal, $PbWO_4$ (PWO) of dimension $2.2\times2.2\times18$ cm^3, coupled to an Avalanche Photo-Diode (APD) and a low-noise preamplifier. The physical and chemical properties of the $PbWO_4$ crystal are given in Table 1.

PWO is a fast scintillating crystal with a rather complex emission spectrum, consisting of two emission components: a blue component peaking at 420 nm (2.9 eV) and a green component peaking at 480-520 nm (2.5 eV). The scintillation characteristics exhibit several

decay time components, the largest (~80%) one being τ ~5 ns. The light yield of this crystal at room temperature is low in comparison with other heavy scintillating crystals (e.g. BGO). However, it depends strongly on temperature. The temperature coefficient is about -2% per ^{o}C in a broad temperature range. At -25 ^{o}C the light yield is increased by about a factor 3 compared to room temperature (20^{o}C), and at the same time, the electronic noise of the photo detector is reduced. Both effects combine to improve the energy resolution. The PHOS will be operated at a temperature of -25^{o}C, which can be easily achieved with standard cooling technology. This temperature must be stabilized to about 0.1-0.2 ^{o}C to keep the light yield and the detector gain constant, with a precision better than 2%.

The use of the lead-tungstate crystal for electromagnetic calorimetry has been extensively studied in recent years [2]. Following a vigorous R&D program launched by the ALICE collaboration, significant progress has been made [3]. We describe hereafter a large PHOS prototype consisting of 256 detection channels, the PHOS-256, together with results of measurements performed with electron and hadron beams at the CERN PS and SPS accelerators.

2 Apparatus

The PHOS-256 consists of 256 detection channels of PWO crystals, assembled as a 16×16 detection matrix. A PWO crystal, coupled to an APD photo-detector integrated with a low-noise preamplifier, constitutes the detection channel. The crystal matrix with the APDs and preamplifiers is contained in a thermo-insulated enclosure and cooled to a temperature of -25 ^{o}C, stabilized with a precision of 0.1 ^{o}C. In addition to the photo-detector, the electronic chain includes a shaping amplifier, analog-to-digital conversion with a buffer memory, and a CAMAC data register read out through a VME front-end processor. The data acquisition system is the ALICE DATE [4] system under Linux, adapted to the PHOS readout configuration. The shaper and the digitizing electronics are mounted outside the cooled enclosure.

An overall monitoring of the detection channels is carried out by a system using light-emitting diodes (LEDs) with stabilized current generators. A charged particle veto (CPV) detector [3] is placed in front of the crystal matrix and completes the PHOS-256 prototype.

2.1 The crystals

The shaped PWO crystals (Fig. 1) of dimension 2.2×2.2×18 cm^3 have been produced by the “North Crystals Co”, Apatity, Murmansk region, Russia. A mass production technology was developed by “North Crystals Co” in cooperation with the Russian Research Centre (RRC) “Kurchatov Institute”, Moscow. The crystals were optically polished. The tolerance in the transverse size was 0, -100 μm, and in length 0, -200 μm. All crystals were certified at the test and certification facility for PWO crystals at the RRC. This facility comprises: a test-bench for the light-yield measurement with a ^{22}Na radioactive source, an optical test-bench for measuring the emission and transmission spectra, a test-bench for measuring the scintillation-light decay time, and equipment for measuring the crystal dimensions.

The light yield and transmission spectrum were measured for every crystal, whereas the emission spectrum and scintillation decay-time spectrum were measured only for a limited sample of crystals. The test-benches were calibrated daily by measuring the one-electron peak position of the photomultiplier, and by measuring the light-yield and transmission spectrum of the reference crystal. These control measurements demonstrated that the absolute precision of the light-yield measurement is about 7%, whereas the precision of the transmission measurement, e.g. at 360 nm and 420 nm, is 0.7% and 0.5% respectively. Only those crystals were accepted which met the following specifications: a light yield at room temperature higher than eight photoelectrons per MeV, a longitudinal inhomogeneity of the light yield lower than 5%, and a transmission at 360 nm, 420 nm and 632 nm higher than 25%, 60% and 70% respectively.

2.2 Detector and readout electronics

2.2.1 Photo-detector and APD high voltage system

Avalanche Photo-Diodes (APD) of type S8148 (S8664-55), produced by Hamamatsu Co, Japan, were used. The advantage of APDs compared to PIN-diodes is that the ‘punch-through’ (or nuclear counter) effect is negligible. This effect is caused by charged particles leaking out through the end of the crystal from incomplete absorption of the electromagnetic shower, causing a large signal in a PIN-diode. For a crystal length of 18 cm this effect becomes significant for energies above 10 GeV.

The S8664-55 APD has an active area of 5×5 mm^2, and is mounted in a ceramic case of 9×11 mm^2. The top surface is protected by a thin epoxy shield. The spectral response exhibits a maximum around 600 nm, with a quantum efficiency around 85%. The gain of an APD increases with decreasing temperature, typically by a factor of 3 at -20 ^oC compared to the gain at 20 ^oC, with a bias voltage of 350 V.

The effective gain of a detection channel depends on a number of factors; the light yield of the PWO crystal, the optical coupling between the crystal and the APD, and in particular the spread in gain factors for a batch of APDs. The distribution of effective gain factors for the channels of the PHOS-256, measured with identical APD bias voltage, is shown in Fig. 2.

The following method was applied in order to equalize the gain factors for the channels of the detection matrix. A batch of APDs were sorted according to the value of the bias voltage corresponding to a gain at room temperature of M=50 at λ=420 nm. Those APDs having close values of bias voltage in the range 350-400V, typically within 2.5 V, formed a group. Then eight APDs were selected from each group, so that 32 different APD groups were used in the PHOS-256. The APDs of a group were biased by the same voltage, so that 32 different values of bias voltages were applied. These bias voltages were obtained by means of 32 resistive dividers connected to a common high voltage power source. The ripple was 7 mV. With this bias voltage system, the spread in effective gain factors for the PHOS-256 channels at a working temperature of -25 ^oC was observed to be of about 20% (RMS).

2.2.2 Preamplifier

A charge-sensitive preamplifier (CSP) on a printed circuit board of area 19×19 mm^2 is mounted to the back side of the APD. The photo-detector and the circuit diagram for the preamplifier are shown in Fig. 3. The preamplifier is an operational amplifier with a feedback capacitance C6 = 1 pF and a field-effect transistor JFET (2SK932) at the input (U1). The characteristics of the JFET determines the preamplifier's noise level and the output rise time. The resistor R28 = 100 MΩ is the direct current feedback and determines the fall time constant of the CPS's output signal, which has been specified to ~100 μs. The base potential of Q6 determines the drain voltage of the JFET (U1) and R23 determines the operating current of U1. The CSP is supplied from +12 V and -6 V with power consumption of 64 mW.

The rise time of the output signal is measured to be 15 - 30 ns depending on the pulse height, and the fall time is around 170 μs. The amplifier gain is designed to be 1V/pC, and measured to be around 0.78 V/pC with RMS noise of ENC = 200-500e, including contributions from the input test signal and measuring device. The rise time is slightly slower than the design specification value. It can be improved to meet the specification value as well as reducing the pulse height dependence, however on the expense of increasing the power consumption by a factor of around 1.6. The final design decisions will be made by taking into account also the heat removal capacity of the PHOS, since the preamplifiers are inside the cold volume.

The design specifications of the CSP are listed in Table 2. The input capacitance of the APD is 80 pF.

2.2.3 Analog shaper

The shaper is a band-pass amplifier designed to match the preamplifier for improving the signal-to-noise ratio and to supply an output pulse shape adapted to the ADC. The shaper circuit diagram and output pulse shape are shown in Fig. 4. The shaper consists of three amplification stages with a gain equal to 7 for each stage. The measured equivalent noise referred to the shaper input is 12 μV RMS. The input differentiation stage includes a pole-zero compensation. For this value the optimum time constants of differentiation and integration are 3.36 μs.

2.2.4 Analog-to-digital conversion and readout

The analog-to-digital conversion is carried out by the chip MAX 198 which is multi-range, fault-tolerant ADC, using successive approximation and internal input track-and-hold circuit to convert the input signal to a 12-bit digital output. The amplitude of the input signal is stored in the S/H circuitry by the signal of a trigger. The S/H outputs are connected sequentially to the input of the 12 bits ADC through an amplifier with programmable gain, and the digitized values are written to a FIFO memory buffer. The control unit sets the addresses for the multiplexer and also stores a gain code which is received from the DAQ program at the start of the measurement. After digitization, the data in the FIFO buffer are read out through a CAMAC register by the VME front-end processor of the DATE DAQ system. The shapers, ADC, memory buffer and interface to the CAMAC register are integrated on a printed circuit board. One board serves 64 crystal channels plus two channels for measuring the temperature

of the matrix. Four such boards are used in the PHOS-256. The digitizer block and readout chain are shown in Fig. 4.

2.3 Mechanical design

A schematic design of the mechanical structure of the PHOS-256 is shown in Fig. 5.

The calorimeter is assembled from detector blocks, *crystal strip units*, each of which comprises eight *crystal detector units* mounted in one row, see Fig. 6. A *crystal detector unit* consists of a PWO crystal, wrapped in Tyvek, coupled to the APD photo-detector which is glued onto the end face of the crystal with an optically transparent compound[1] having a refractive index (1.7) close to that of the crystal. The compound transmission spectrum matches the lead-tungstate crystal emission spectrum, as well as the APD quantum efficiency.

Since the PHOS-256 operates with the crystals at a temperature of –25°C, the mechanical structure is separated by thermo-insulation into two enclosures, cold and warm. The crystal detector units are located in the cold volume, whereas the readout electronics is mounted outside in the warm area.

The PHOS-256 with the CPV and a front view of the crystal matrix are shown in Fig. 7.

2.4 Cooling

The cooling and thermo-stabilization system was developed specially for the PHOS-256. A block and control diagram of the system is shown in Fig. 8.

The side walls of the cold volume are equipped with cooling panels, and heat is removed by a liquid coolant (Hydrofluoroether[2]) pumped through the channels in these panels. The coolant is transported over a distance of a few meters between the detector and the cooling device, which is a one-stage freon refrigerating machine[3], operating with a refrigerant of type R404A. The crystal temperature is stabilized with a precision of 0.1 to 0.2°C by means of a temperature control system, which consists of two sub-systems. The first one controls the cooling system and has the following functions: measurement of the ambient temperature, measurement of the temperatures of the coolant at the output of the heat exchanger and at the

1. Meltmount Quick-Stick, delivered by Cargille Labs, USA
2. HFE-7100, 3M Industry Co, USA
3. Produced by GELPHAFRED Co, Spain, of type 15X-GK-47.5

input and output of the cooling panels, measurement of the coolant level, control of the pump, control of the compressor, control of a special additional heater of the coolant, and the emergency control of the coolant level. The second sub-system monitors the crystal array temperature and the temperature in the warm area. The coolant temperature at the output of the heat exchanger is measured by means of thin commercial semiconductor sensors. The coolant temperature at the input of the cooling panels is measured by means of a highly stable platinum sensor. For measurement of the crystal array temperature, eight special thermo-resistive nickel sensors with thickness of 50 μm are used, some inserted in the gap between crystals, and others glued onto the flat surfaces (Fig. 9). The acquisition of the monitoring data and the control of the cooling system performance are carried out by means of a control system based on a PC with interface electronics. In addition, temperature measurement data from two sensors in the crystal array were included in the event data and recorded by the DAQ system.

The performance of the cooling and thermo-stabilization system was evaluated during the beam tests. The crystal volume was cooled down to -25^{o}C, with the APDs and preamplifiers powered. The time needed to reach a stable temperature state was about 50 h. During the beam test period the temperature in the experimental area oscillated by up to 10^{o}C over a 24h period. The temperatures at the measuring points of the crystal matrix are plotted versus time in Fig. 9. The variation of the crystal temperature is within 0.1^{o}C. The temperature differences between crystals located in different positions of the matrix did not exceed 1.5^{o}C.

2.5 LED monitoring system

In addition to the preamplifier calibration inputs, all PHOS-256 detection channels are monitored by a system using light emitting diodes (LEDs) with stabilized current generators.

The LED Monitoring System (MS) consists of a Master Module (MM) and a Control Module (CM). The MM, located in the counting room, is a CAMAC module whose functions are implemented in FPGAs. The MM contains a CAMAC function decoder, memory units with active channel addresses and channel amplitudes, and control and protocol logic. The CM board is located in the cold volume of the PHOS-256, directly over the crystal faces, and is a 16×16 matrix of super bright green LEDs[1]. The intensity of the light flash is controlled by 8-bit DACs of type AD5300BRT[2]. All LED's, current generators, control and decoding circuits of

1. L934SGC, Kingbright Electronic Co. Ltd
2. From Analog Devices

the CM board are mounted on one PCB. The CM is connected to the MM with a flat twisted-pair cable. The monitoring system is controlled by a dedicated host computer connected to the MM through CAMAC. The communication between the MM and the CM is based on the SPI protocol.

The measured long-term stability of the channel monitoring is 1.2×10^{-3} [5].

The monitoring system can be enabled for different operational modes, such as the passive mode used during the beam test. In this mode the system is activated by special external triggers generated between the beam spills.

3 Beam tests

Extensive tests of the PHOS-256 were carried out at the CERN PS and SPS beam lines T10 and X5 with electron and pion beams in an momentum range from 0.6 to 150 GeV/c. The beam momentum spread was about 1%. A typical beam intensity was 2.5×10^3 particles per spill for the calibration runs and 2×10^4 negative pions per spill for neutral pion measurements.

3.1 Experimental set-ups, beam-line counters and triggers

The experimental set-ups, the trigger conditions and the trigger counter set-ups were similar for both the SPS and PS tests. The layout of the PS beam test with electron beam is illustrated in Fig. 10.

The PHOS-256 was installed on a remotely controlled movable platform, which enabled the crystal matrix to be scanned horizontally and vertically by the beam. The crystal inclination angle could be changed by means of wedges to make measurements at different incident angles. A set of thin scintillator beam-counters and a gas Cherenkov-counter were installed upstream of the detector. A set of two Narrow Beam detectors, S_f, was placed at a distance of 5 cm in front of the detector. The transverse beam size defined by means of these detectors was 1.0×1.0 cm^2. The position of the beam particle on the front face of the crystal array was measured by a delay-line wire chamber (DWC) with a precision of 0.3 mm in both x and y directions.

A set of possible trigger combinations and the trigger logic is listed in Fig. 10. To control the pedestals of the ADCs and the channel amplification of the electronics, pulser, pedestal and LED triggers were generated between beam spills from the accelerator. In order to distribute the signal from a master pulse generator to all preamplifiers without introducing external cabling, a precision fan-out system was integrated in close vicinity to the crystal array.

In Fig. 11 the layout of the beam test with the pion beam is shown. In this case, the decay photons from neutral pions produced in interactions of charged pions with light nuclei were measured under the requirement that no charged particle hits the detector. Therefore, a reaction trigger was used which consisted of two counters in front of the target and a plastic scintillator veto detector in front of the PHOS-256. The trigger logic is shown in Fig. 11.

3.2 Experimental details

Two different experiments have been carried out: a beam energy scan to measure the energy resolution and linearity of the PHOS-256, and a measurement of neutral pions produced in inclusive reactions of charged pions with light nuclei, e.g. $\pi^- + {}^{12}C \rightarrow \pi^0 + X$.

Beforehand, relative calibration of the detector channels was performed. Two different methods were used: i) calibration with Narrow Electron (NE) beam, and ii) calibration with Wide Electron (WE) beam. For the first method, the crystal was aligned to the beam line and selected by the trigger counters. A calibration run with 1×10^3 events was accumulated for each crystal. The events were taken with the NE trigger at 50 GeV at the X5 beam and at 2 GeV at the T10 beam. Only the 60 crystals at the periphery of the matrix were calibrated with this method, because a calibration of all 256 crystals with the NE beam would have been too time consuming. With the WE beam, the beam was spread over an area of 10×10 cm^2, so that during one calibration run 4×4 crystals were irradiated simultaneously with approximately the same number of electrons.

After calibrating, energy scans were performed for 16 different zones of 3×3 crystals, with the beam aligned to the center crystal. At the SPS the energy scan spanned 10 - 150 GeV, and at the PS from 0.6 GeV to 5 GeV. During the energy-scan runs the collimator slits were almost closed for an optimal energy definition.

The neutral meson measurements were carried out at the PS T10 beam-line. For these measurements a plastic target of thickness 8 cm and an aluminum target of thickness 2.5 cm

were irradiated with 6 GeV/c π^- mesons. The beam intensity was ~10^4 mesons per spill, which generated about 30 neutral triggers per spill. The targets were located either at 1.22 m or 0.81 m from the front face of the crystal matrix. These two distances enabled to collect samples with statistically significant data for both π^0 and η mesons.

4 Analysis of the experimental data

The data analysis starts with the relative calibration of the detector channels. A preliminary gain adjustment was achieved and calculated by means of the pulser signals in each detector channel.

For data taken with the NE beam, the electron peak position was calculated for each detector channel from a Gaussian fit to the recorded amplitude distribution. An example of such a fit is shown in Fig. 12C. The histograms were filled only at NE triggers, i.e. a hit within the 1.0×1.0 cm^2 area of the S_f counters. From the data taken with pulser and pedestal triggers, the positions and the corresponding widths (σ_{puls} & σ_{ped}) of the pulser and pedestal signals were calculated. Examples of single-channel amplitude distributions are shown in Fig. 12A, B and C for different types of triggers. The electron peak positions, measured at the same energy in each detector, were then aligned relative to each other by introducing a set of inter-calibration constants. These constants are calculated as ratios of the peak position in the crystal which was chosen as a reference crystal to the peak positions in each crystal. After the relative calibration, the total energy deposited by the electromagnetic shower in the crystal(s) can be calculated. The deposited energy is obtained by summing the signals surpassing the pedestal values in the inner nine (3×3) crystals. An example of how the sum of the nine central crystals is distributed for electrons at beam energy 2 GeV, is shown in Fig. 12 part D. A Gaussian shape was fitted to the measured distribution over a range of $\pm 2\sigma$ around the peak position. The absolute normalization factor was deduced by comparing the summed peak position and the beam energy.

For data taken with the WE beam, the absolute gain factors α_i for all the channels were calculated by fitting a Gaussian distribution to the summed signals in all the crystals at the calibration energy E_e, by means of minimization of the function:

$$F(\alpha) = \sum_{j=1}^{N} \left(\sum_{i} \alpha_i A_{ij} - E_e \right)^2 ,$$

where the index *i* runs over crystals with amplitude over the detector threshold, and index *j* runs over all calibration events.

The absolute gain factors obtained with the two methods are in a good agreement with each other.

4.1 System stability

To check the stability of the system, the positions and widths (σ_{ped} & σ_{puls}) of the pedestal and pulser signals were checked throughout the data-taking periods. As an example, the values of the pedestal and the pedestal width (σ_{ped}) for the reference crystal, during one of the calibration experiments, are shown in Fig. 13.

4.2 Energy resolution and linearity curves

The measured linearity curve, i.e. the nominal beam energy versus the position of the peaks in ADC channels multiplied by the absolute gain factors found in the calibration, is shown in Fig. 14 for one of the 3×3 detector arrays. As seen from this figure, the detector response in the energy range from 0.4 to 150 GeV is constant with a precision better than 1%.

The energy resolution at different beam energies was determined from a Gaussian fit to the electron peaks obtained by summation of the gain corrected signals in the crystals of the 3×3 detector array around a given central crystal. The distributions of the energy resolution values for 16 different 3×3 detector arrays are shown in Fig. 15. These results demonstrate that the channel gains are rather uniform. The value averaged over the 16 arrays versus the electron beam energy is shown in Fig. 16. No correction for the beam momentum spread has been applied.

The energy resolution of an electromagnetic calorimeter can be parametrized as

$$\frac{\sigma_E}{E} = \sqrt{\left(\frac{a}{E}\right)^2 + \left(\frac{b}{\sqrt{E}}\right)^2 + c^2}$$

where the energy E is in GeV, a represents the noise, b represents the stochastic term, and c represents the constant term. The stochastic term b takes into account the fluctuations in the electromagnetic shower and variations due to photoelectrons statistics, which includes, in particular, the light yield contribution and the APD excess noise factor. The term a includes contributions from preamplifier noise, digitalization noise, and, in principle, pile-up noise, the latter being negligible in our tests. The constant term takes into account shower leakage at the back end of the crystals, inter-calibration errors, non-uniformity in the light collection and geometrical effects.

The parameters obtained by fitting the equation to the data are listed in Fig. 16.

4.3 Two-photon invariant mass spectrum

In the tests with charged pion beams, data were taken to identify π^0 and η mesons. A typical single event display showing the two-dimensional pattern of crystals with non-zero energy deposition is shown in Fig. 17.

As seen in the figure, several showers can be identified in a single event. Pairs of showers can result from the $\gamma\gamma$ decay of a neutral meson (π^0 or η) produced in a reaction of a charged pion with a target nucleus. An invariant mass spectrum of all photon pairs in these events are shown in Fig. 18. Only non-overlapping clusters have been considered.The π^0 and η peaks are clearly seen on top of the combinatorial background. The peaks were fitted with Gaussian distributions together with two 3rd order polynomials representing the backgound. Peak positions at 135.9±0.2 MeV/c^2 for π^0 and 544±2 MeV/c^2 for η were found. Invariant mass resolution of 8.39±0.21 MeV/c^2 and 17.6±2.3 MeV/c^2 were obtained for π^0 and η, respectively.

5 CONCLUSIONS

A large-scale prototype with 256 detector channels of the ALICE/PHOS electromagnetic spectrometer has been developed and tested. The detector channel is a $PbWO_4$ crystal coupled to an APD with a low-noise preamplifier. The prototype comprises the following subsystem: front-end electronics, a cooling and thermo-stabilization system, a light-emitting diode monitoring system, and a charged particle veto detector. The prototype operates at a temperature of -25 ^{o}C stabilized to better than 0.1 ^{o}C.

The prototype has been tested with electron and pion beams at the CERN PS and SPS accelerators. In the tests with the electron beam, energy resolution and linearity have been measured over a broad energy domain ranging from 0.6 to 150 GeV. Neutral pions as well as η - mesons, produced in the inclusive reactions $\pi^- + {}^{12}C \rightarrow \pi^0 + X$ and $\pi^- + {}^{12}C \rightarrow \eta + X$, have been measured at various energies.

The measured energy resolution for a 3x3 detector array is parametrized as

$$\frac{\sigma_E}{E} = \sqrt{\left(\frac{a}{E}\right)^2 + \left(\frac{b}{\sqrt{E}}\right)^2 + c^2}$$

where the energy E is in GeV, a = 0.0130±0.0007 GeV (i.e. 4.3 MeV/channel), b=0.036±0.002 sqrt(GeV), and c=1.12±0.3%.

The mass resolution is 8.39 MeV for π^0 and 17.6 MeV for η.

References

[1] ALICE Collaboration, Technical Proposal, CERN/LHCC 95-71 (1995) - URL: https://edms.cern.ch/document/316077/1, and Addendum to ALICE Technical Proposal, CERN/LHCC 96-32 (1996) - URL: https://edms.cern.ch/document/316523/1.

[2] Results of recent developments in this field can be found in: i) Proceedings of the Seventh International Conference on Inorganic Scintillators and their Use in Scientific and Industrial Applications, (SCINT2003), Valencia, Spain, 8-12 September, 2003, Nuclear Instruments and Methods in Physics Research A, article in Press (Available online 25 August 2004); ii) Proceedings of the FINUPHY Workshop on Advanced Electromagnetic Calorimetry and its Applications (FEMC03), March 10/11, 2003, Jülich, Germany (not yet published); iii) Proceedings of the 6th International Conference on Inorganic Scintillators and their Use in Scientific and Industrial Applications (SCINT2001), Chamonix, France, September 16-12, 2001, Nuclear Instruments and Methods in Physics Research A, vol. 486, Issues 1-2, 21 June 2002; iv) Proceedings of the International Workshop on Tungstate Crystals, Rome, October 12-14, 1998, ISBN 88-87242-10-0; v) Proceedings of the "KEK-RCNP International School and mini-Workshop for Scintillating Crystals and their Applications in Particle and Nuclear Physics", Nov. 17-18, 2003, KEK, Japan (not yet published).

[3] ALICE Collaboration, Technical Design Report of the Photon Spectrometer (PHOS), CERN/LHCC 99-4, March 1999 - URL: https://edms.cern.ch/document/398934/1.

[4] ALICE Technical Design Report of the Trigger, Data Acquisition, High-Level Trigger and Control System, CERN-LHCC-2003-062 - URL:https://edms.cern.ch/document/456354/1

[5] A.M. Blik, M.Yu. Bogolyubsky, S.V. Erin, et al., Pribory i Tehnika Experimenta 2003, N6, pages 1-6.

Tables

Table 1: $PbWO_4$ properties

Density (g/cm^3)	8.28
Radiation length (cm)	0.89
Interaction length (cm)	19.5
Moliere radius (cm)	2.0
Melting point (^oC)	1123
Hardness (Moh)	4
Refractivity index along ξ axis (λ = 632 nm)	2.16
Hygroscopicity	None
Chemical activity	Inert

Table 2: Design specifications for PHOS preamplifier

Sensitivity with C_{fc} = 1 pF	1 V/pC
Maximum charge	8 pC
Noise	ENC = 290e^- + 1.8 (e^-/pF) × C_{APD}(pF)
Rise time	t_F = 5 ns + 0.07 (ns/pF) × C_{APD}(pF)
With C_{APD} = 80 pF : Noise Rise time	 460 e^- 15 ns
Output dynamic range	1 mV to 8 V
Power	+12 V, -6 V
Power consumption	64 mW

Figure captions

Figure 1: PHOS $PbWO_4$ crystal. Courtesy: CERN Photo Lab.

Figure 2: Distribution of relative channel gains at working temperature -25 ^{o}C with APD bias voltage of 400 V.

Figure 3: Photodetector assembly: top - APD and preamplifier, bottom - circuit diagram of preamplifier.

Figure 4: Front-end electronics and readout chain: A - shaper circuit diagram, B - output pulse shape, C - digitizer block, D - complete chain.

Figure 5: Mechanical design of the PHOS-256 calorimeter prototype.

Figure 6: The *crystal strip unit*.

Figure 7: The PHOS-256 calorimeter: A - detector and cooling system, B - closed detector with CPV on top, C - crystal matrix, D - close-up of the CPV.

Figure 8: Block diagram of the cooling/thermo-stabilization system.

Figure 9: Temperature measurements on the crystal matrix. Top - placement of sensors, bottom - crystal temperatures and external temperature vs. time.

Figure 10: Experimental set-up and trigger conditions for the test of the PHOS-256 with the electron beam.

Figure 11: Experimental set-up and trigger conditions for the test of the PHOS-256 with the pion beam.

Figure 12: Examples of spectra obtained during the electron beam test with different kinds of triggers: A - pedestal, B - pulser, C - central detector at *NE* trigger, D - 3×3 sum.

Figure 13: Pedestal position and width as function of run number.

Figure 14: Linearity curve, 0.5-150 GeV, ratio to beam energy, logarithmic energy scale.

Figure 15: The distribution of energy resolution measured for 16 different 3×3 arrays of the PHOS-256 at 2.5 and 60 GeV electron energy.

Figure 16: Average energy resolution vs. electron energy, over 16 different 3×3 arrays.

Figure 17: ADC pulse height distribution for the inclusive 70 GeV/c $\pi^- + {}^{12}C \rightarrow \pi^0 + X$ reaction. Each square corresponds to the response of a single detector channel.

Figure 18: The invariant mass spectra from the inclusive reaction 6 GeV/c $\pi^- + {}^{12}C \rightarrow \pi^0 + X$, measured at a distance of 122 cm. The solid line is a fit of Gaussians plus 3rd order polynomials.

Figures

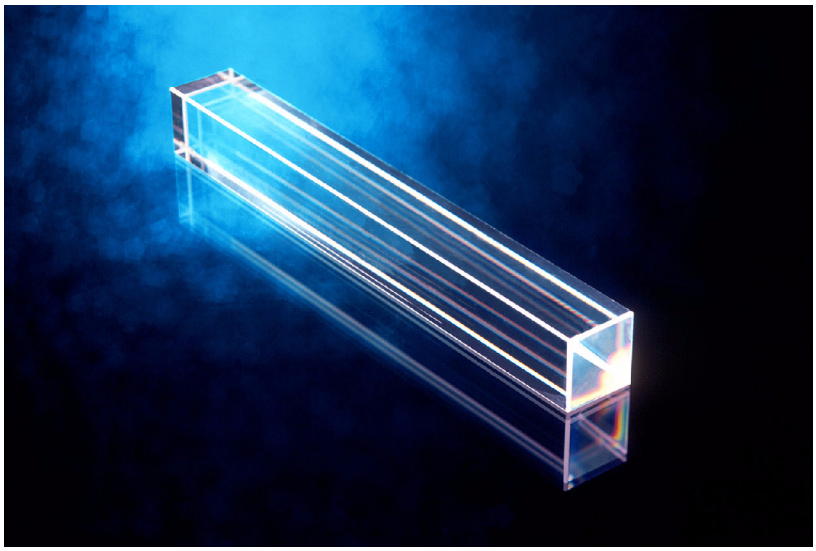

Fig. 1

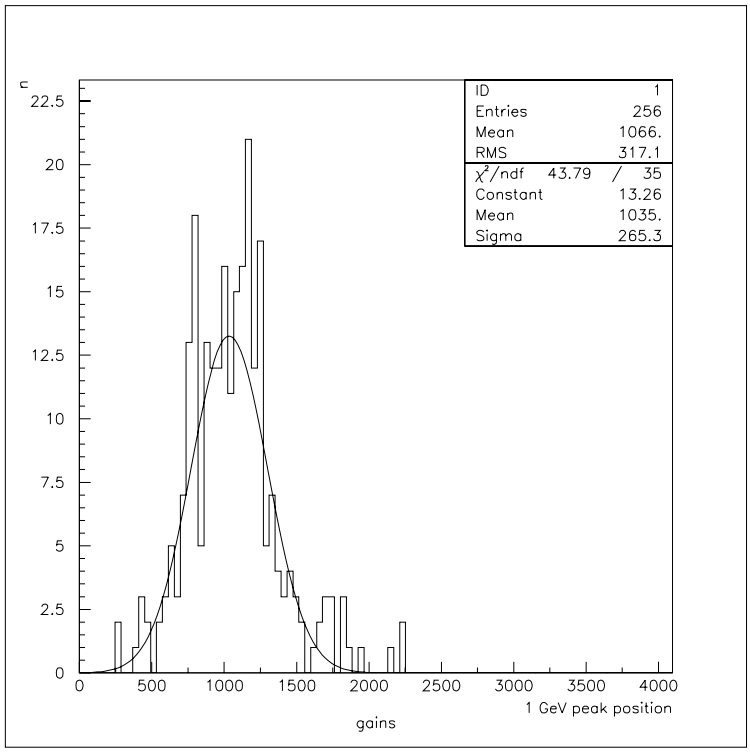
ID 1
Entries 256
Mean 1066.
RMS 317.1
χ²/ndf 43.79 / 35
Constant 13.26
Mean 1035.
Sigma 265.3
22.5
20
17.5
15
12.5
10
7.5
5
2.5
0
0 500 1000 1500 2000 2500 3000 3500 4000
gains
1 GeV peak position

Fig. 2

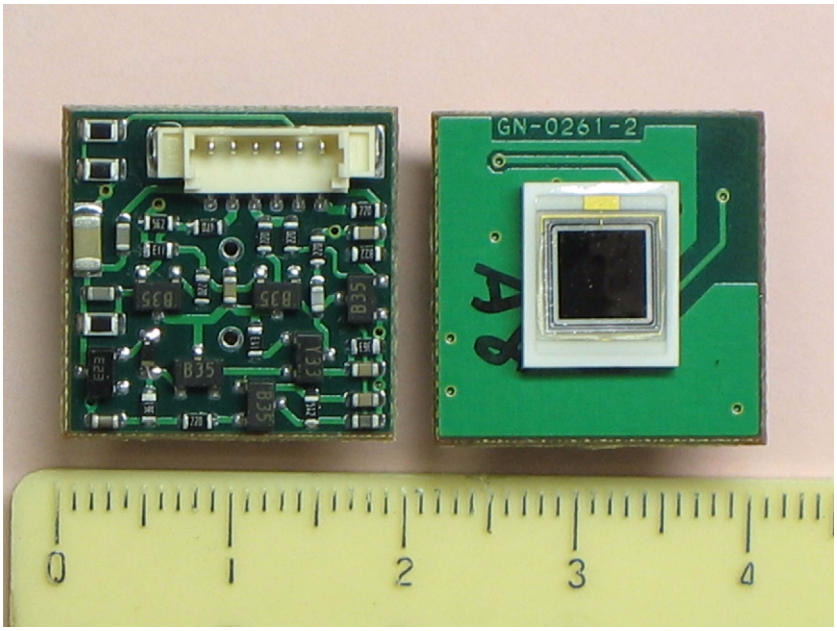
GN-0261-2
0
1
2
3
4

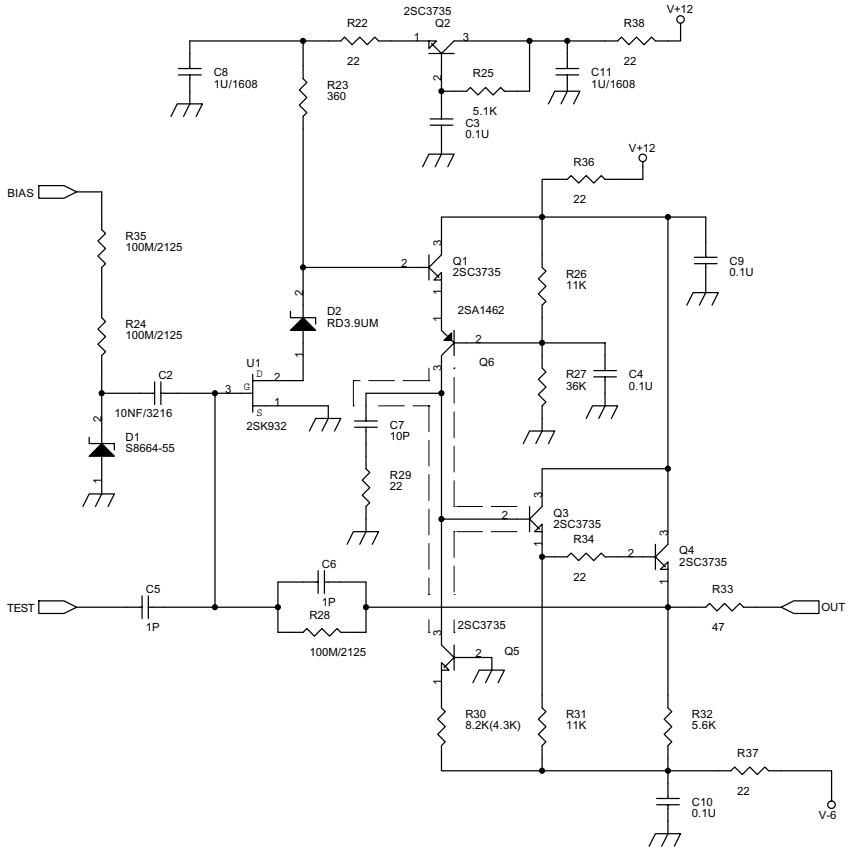
2SC3735
Q2
R22
22
R38
22
V+12
C8
1U/1608
R23
360
R25
5.1K
C3
0.1U
C11
1U/1608
V+12
R36
22
BIAS
R35
100M/2125
R24
100M/2125
Q1
2SC3735
R26
11K
C9
0.1U
D2
RD3.9UM
2SA1462
Q6
U1
C2
10NF/3216
D1
S8664-55
2SK932
R27
36K
C4
0.1U
C7
10P
R29
22
Q3
2SC3735
R34
22
Q4
2SC3735
C6
1P
R28
100M/2125
C5
1P
TEST
R33
47
OUT
2SC3735
Q5
R30
8.2K(4.3K)
R31
11K
R32
5.6K
R37
22
C10
0.1U
V-6

Fig. 3

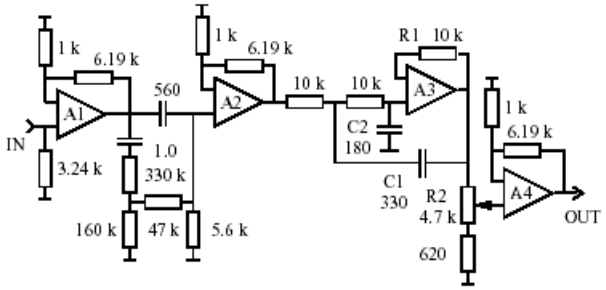
1 k
6.19 k
1 k
6.19 k
R1 10 k
560
10 k
10 k
A1
A2
A3
IN
C2
180
1 k
6.19 k
3.24 k
1.0
330 k
C1
330
R2
4.7 k
A4
OUT
160 k
47 k
5.6 k
620

A

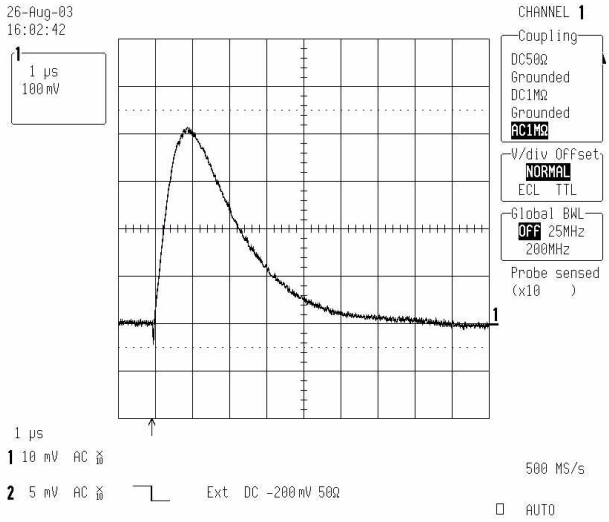
26-Aug-03
16:02:42
1 µs
100 mV
CHANNEL 1
Coupling
DC50Ω
Grounded
DC1MΩ
Grounded
AC1MΩ
V/div Offset
NORMAL
ECL TTL
Global BWL
Off 25MHz
200MHz
Probe sensed
(x10)
1 µs
1 10 mV AC
2 5 mV AC
Ext DC -200mV 50Ω
500 MS/s
AUTO

B

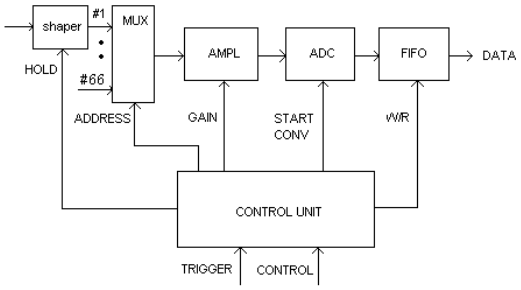
shaper
#1
MUX
HOLD
#66
ADDRESS
AMPL
ADC
FIFO
DATA
GAIN
START
CONV
WR
CONTROL UNIT
TRIGGER
CONTROL

C

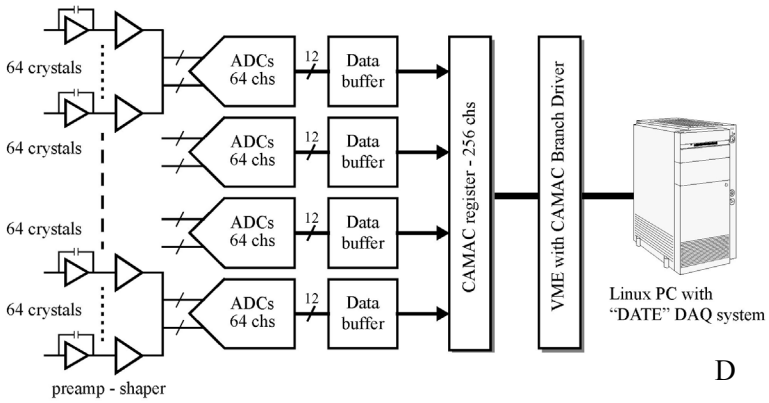
64 crystals
64 crystals
64 crystals
64 crystals
ADCs
64 chs
12
Data
buffer
CAMAC register - 256 chs
VME with CAMAC Branch Driver
Linux PC with
"DATE" DAQ system
preamp - shaper

D

Fig. 4

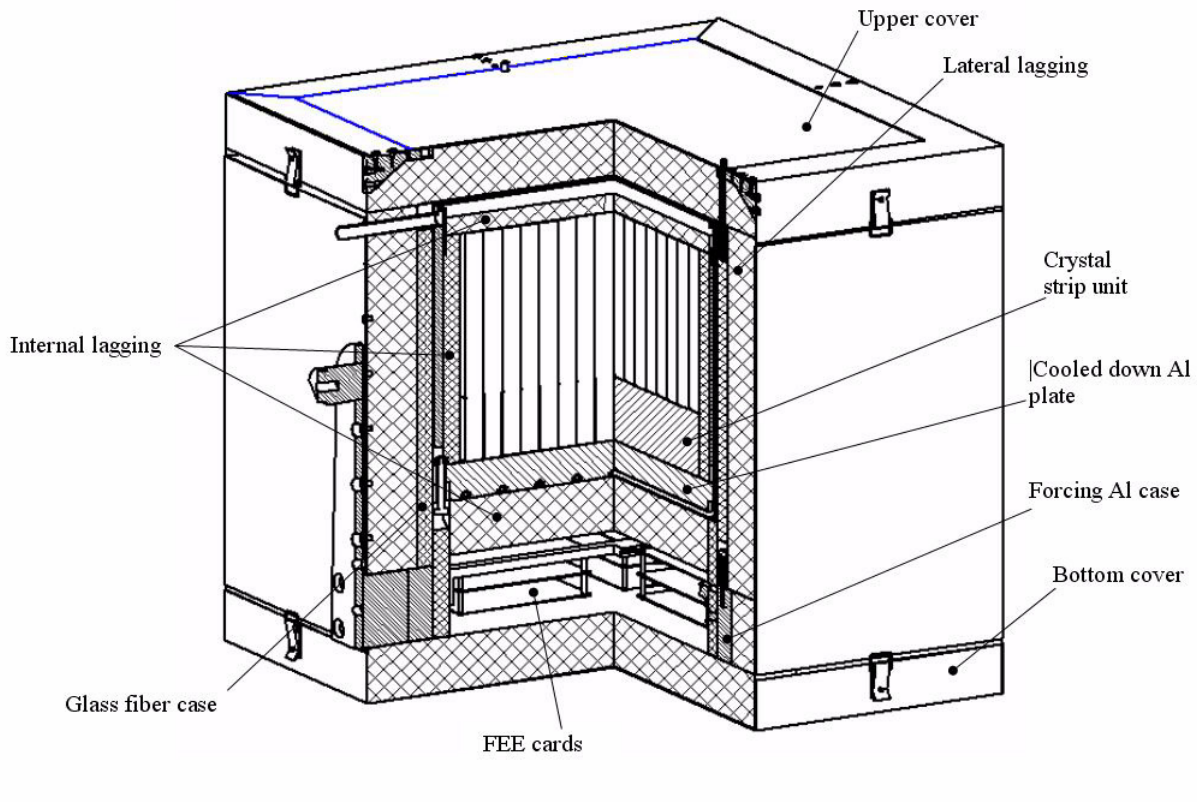
Upper cover
Lateral lagging
Crystal strip unit
Internal lagging
Cooled down Al plate
Forcing Al case
Bottom cover
Glass fiber case
FEE cards

Fig. 5

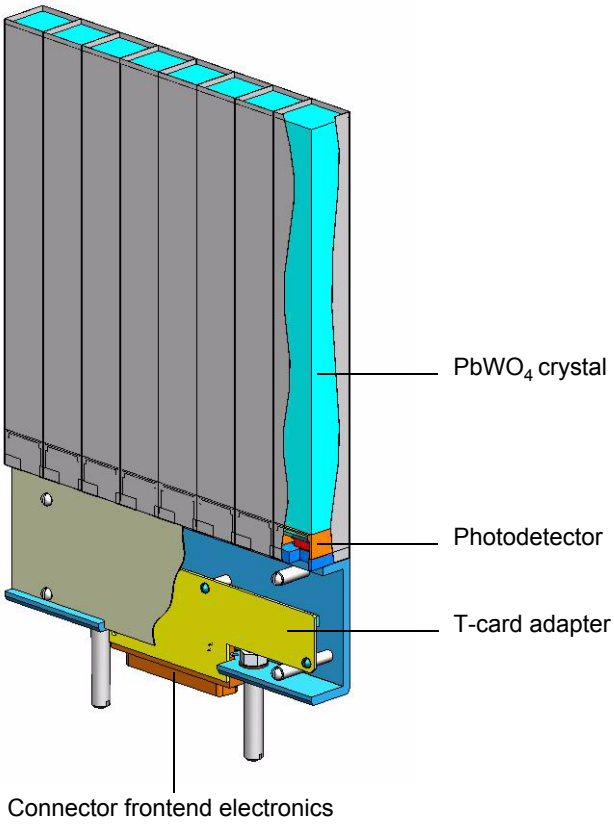
PbWO4 crystal
Photodetector
T-card adapter
Connector frontend electronics

Fig. 6

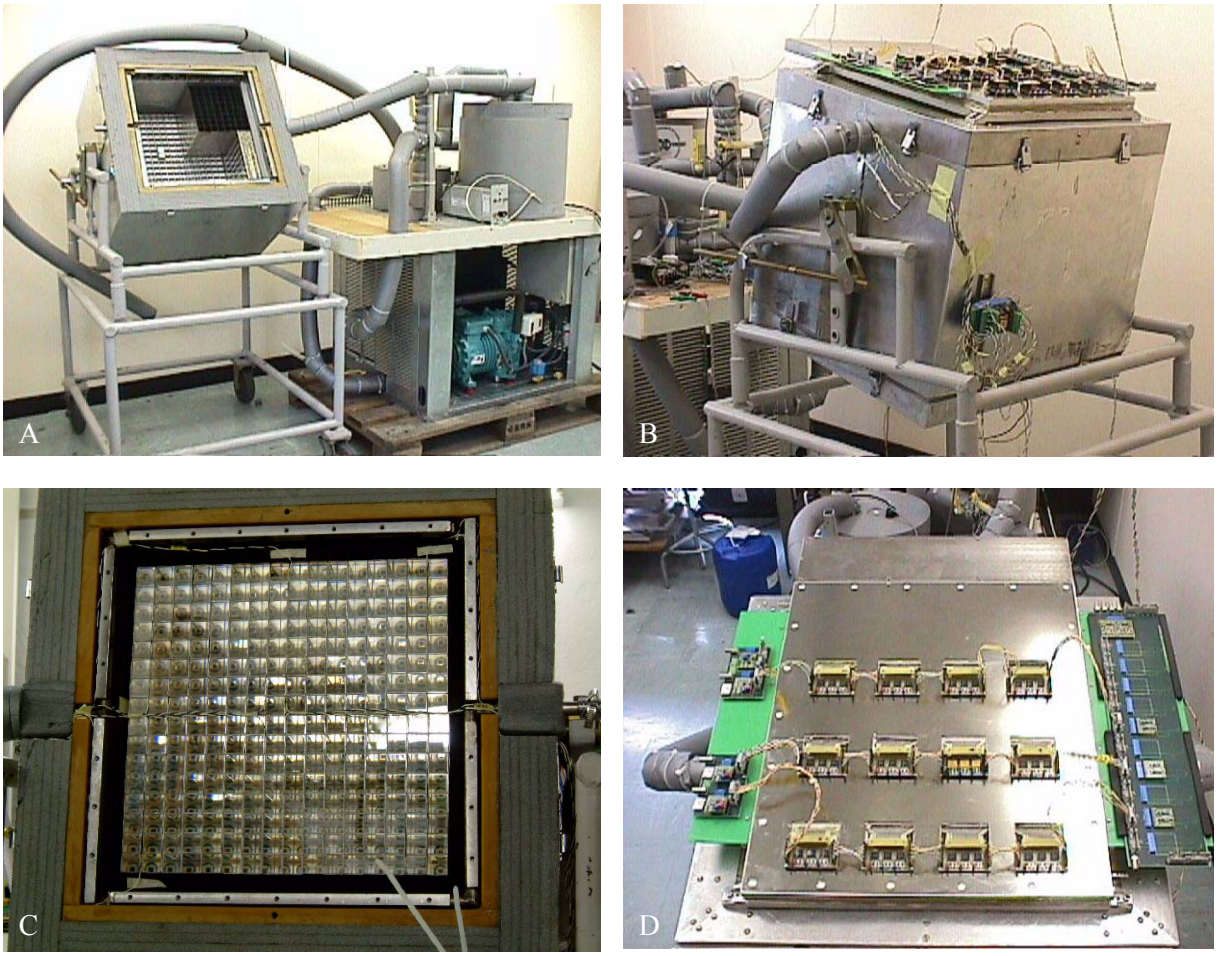

Fig. 7

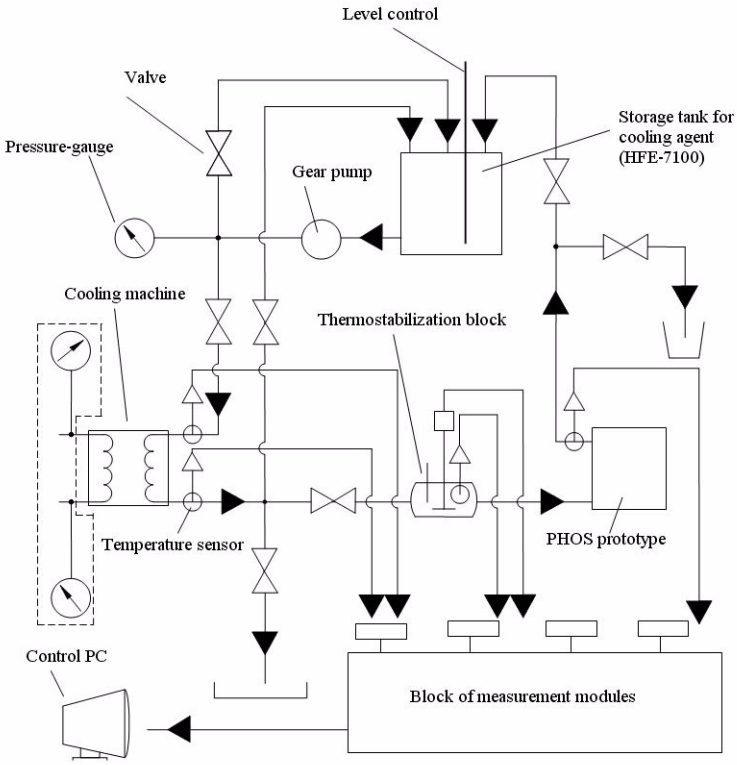
Level control
Valve
Pressure-gauge
Gear pump
Storage tank for cooling agent (HFE-7100)
Cooling machine
Thermostabilization block
Temperature sensor
PHOS prototype
Control PC
Block of measurement modules

Fig. 8

Thin thermo-resistive nickel sensor

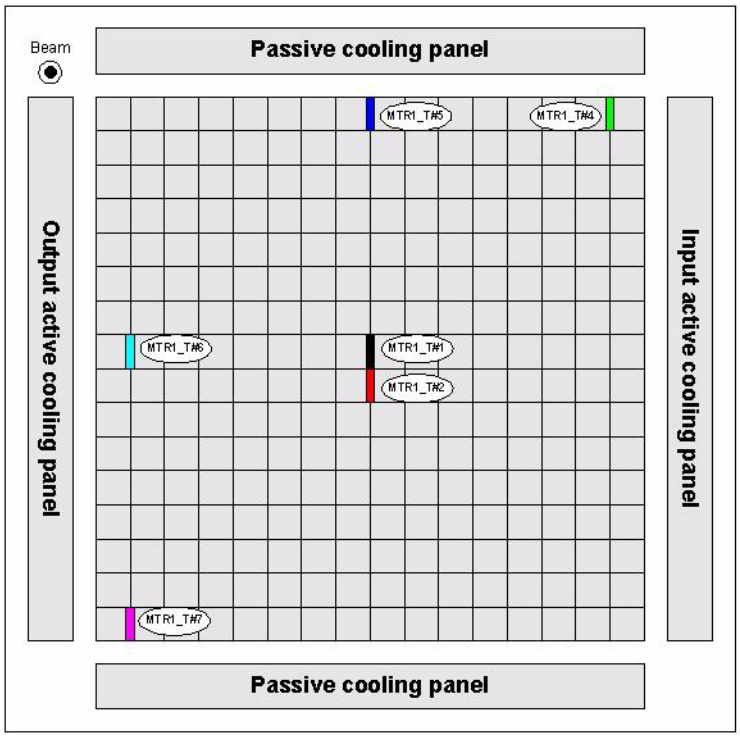

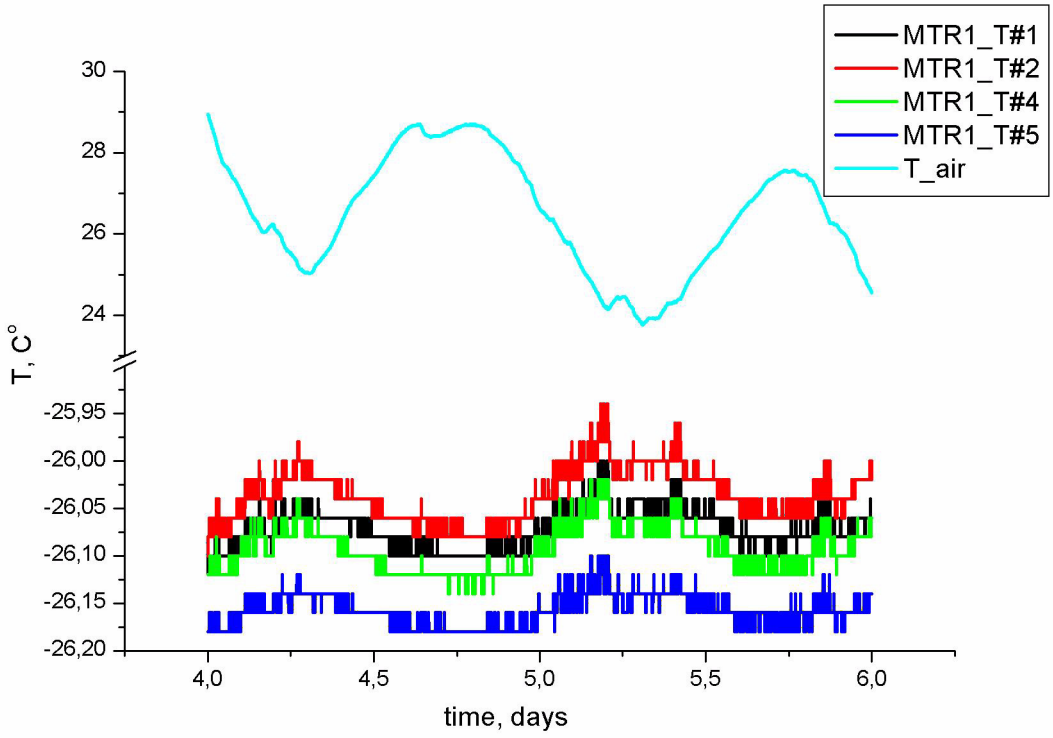

Fig. 9

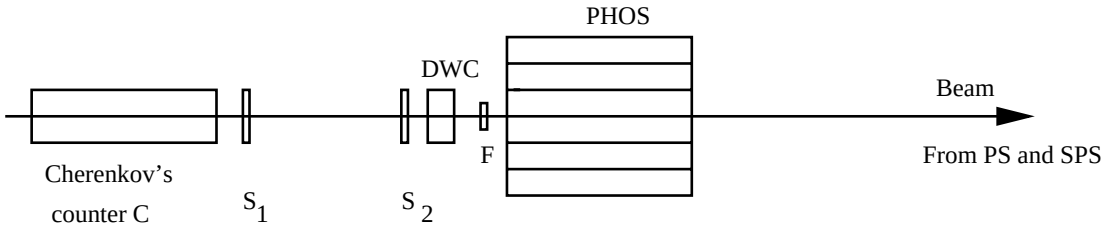

Trigger combinations:

S_1 x S_2 x C − wide Electron (WE)

S_1 x S_2 x C x F −narrow Electron (NE)

Fig. 10

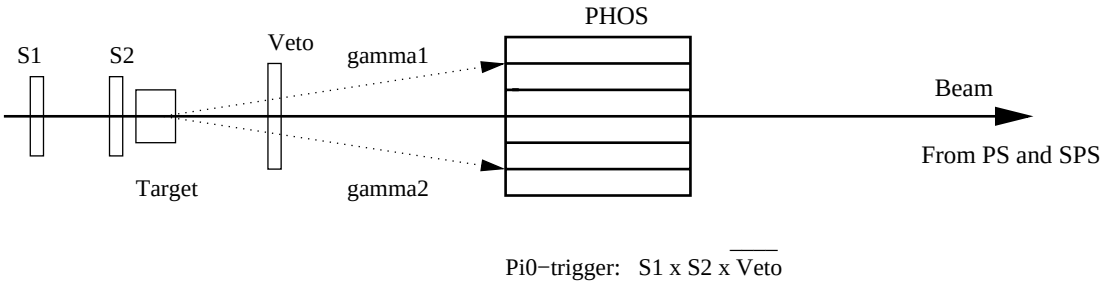
PHOS
S1
S2
Veto
gamma1
Beam
From PS and SPS
Target
gamma2
Pi0−trigger: S1 x S2 x Veto

Fig. 11

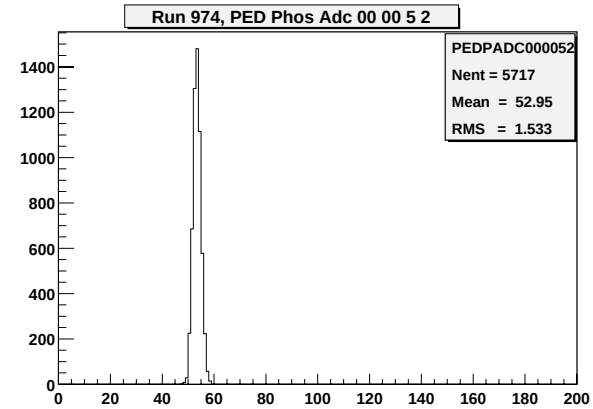
Run 974, PED Phos Adc 00 00 5 2
PEDPADC000052
Nent = 5717
Mean = 52.95
RMS = 1.533

A

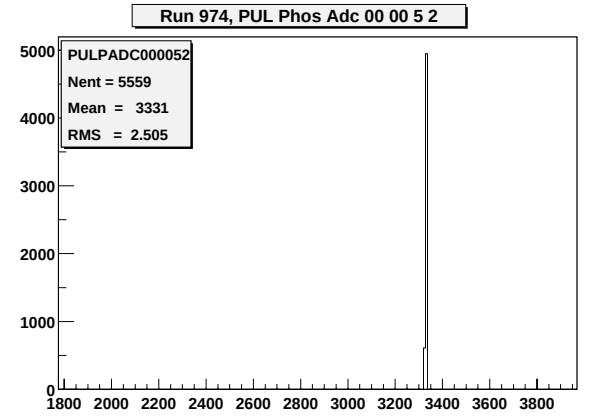
Run 974, PUL Phos Adc 00 00 5 2
PULPADC000052
Nent = 5559
Mean = 3331
RMS = 2.505

B

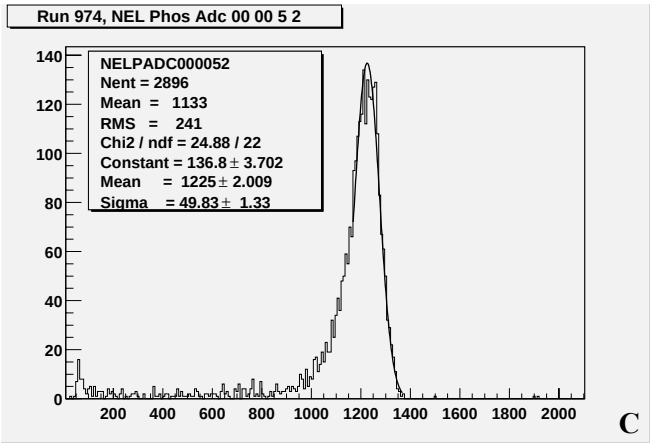
Run 974, NEL Phos Adc 00 00 5 2
NELPADC000052
Nent = 2896
Mean = 1133
RMS = 241
Chi2 / ndf = 24.88 / 22
Constant = 136.8 ± 3.702
Mean = 1225 ± 2.009
Sigma = 49.83 ± 1.33

C

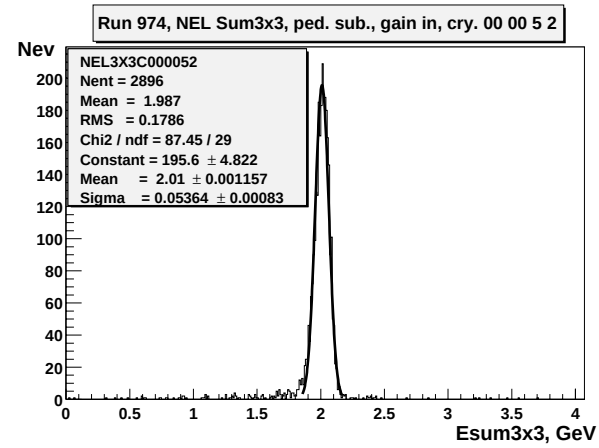
Run 974, NEL Sum3x3, ped. sub., gain in, cry. 00 00 5 2
Nev
NEL3X3C000052
Nent = 2896
Mean = 1.987
RMS = 0.1786
Chi2 / ndf = 87.45 / 29
Constant = 195.6 ± 4.822
Mean = 2.01 ± 0.001157
Sigma = 0.05364 ± 0.00083
Esum3x3, GeV

D

Fig. 12

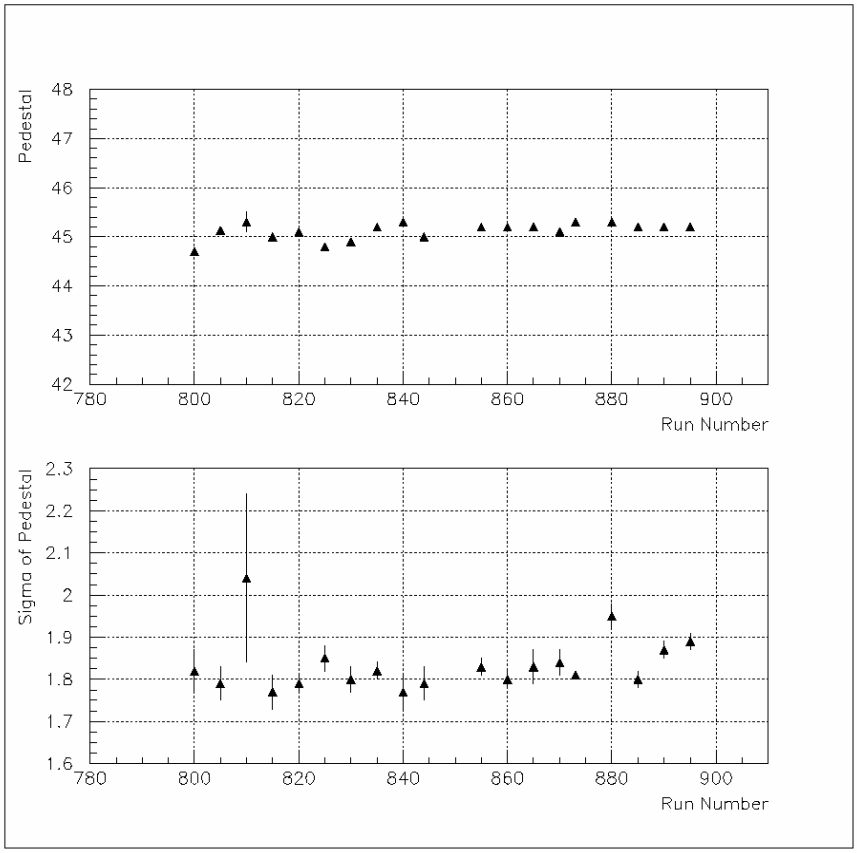
Pedestal
48
47
46
45
44
43
42
780
800
820
840
860
880
900
Run Number
Sigma of Pedestal
2.3
2.2
2.1
2
1.9
1.8
1.7
1.6
780
800
820
840
860
880
900
Run Number

Fig. 13

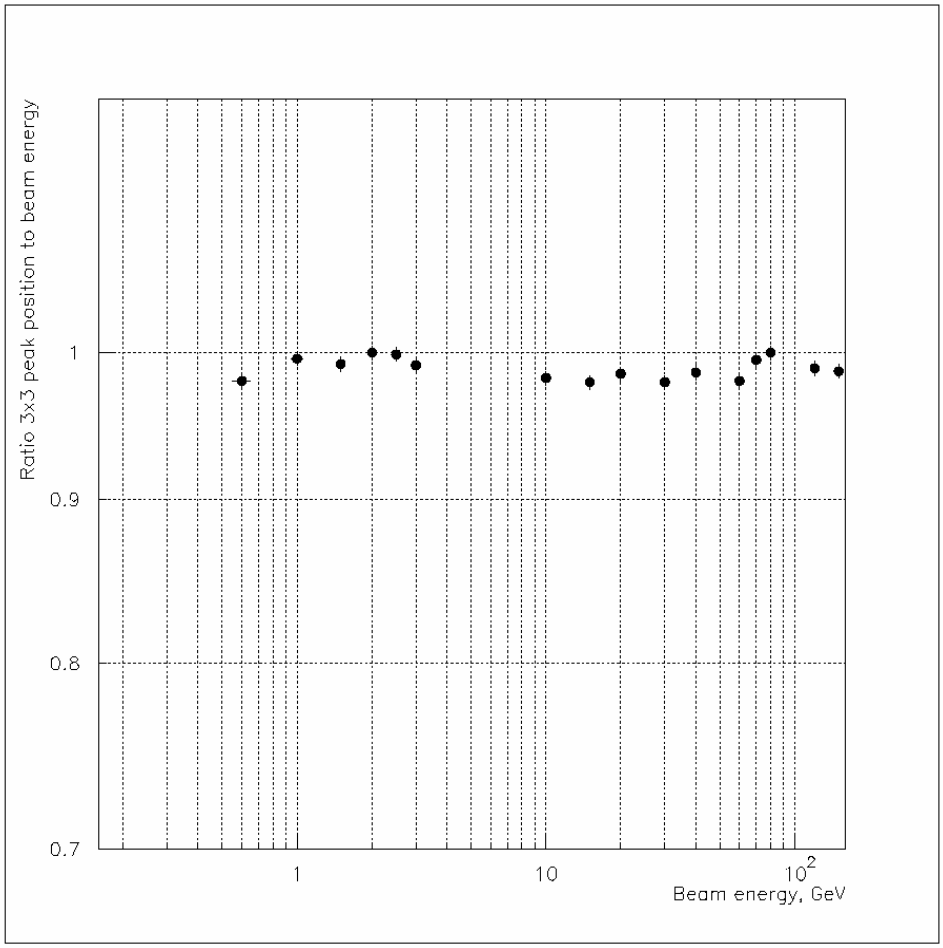
Ratio 3x3 peak position to beam energy
1
0.9
0.8
0.7
1
10
10^2
Beam energy, GeV

Fig. 14

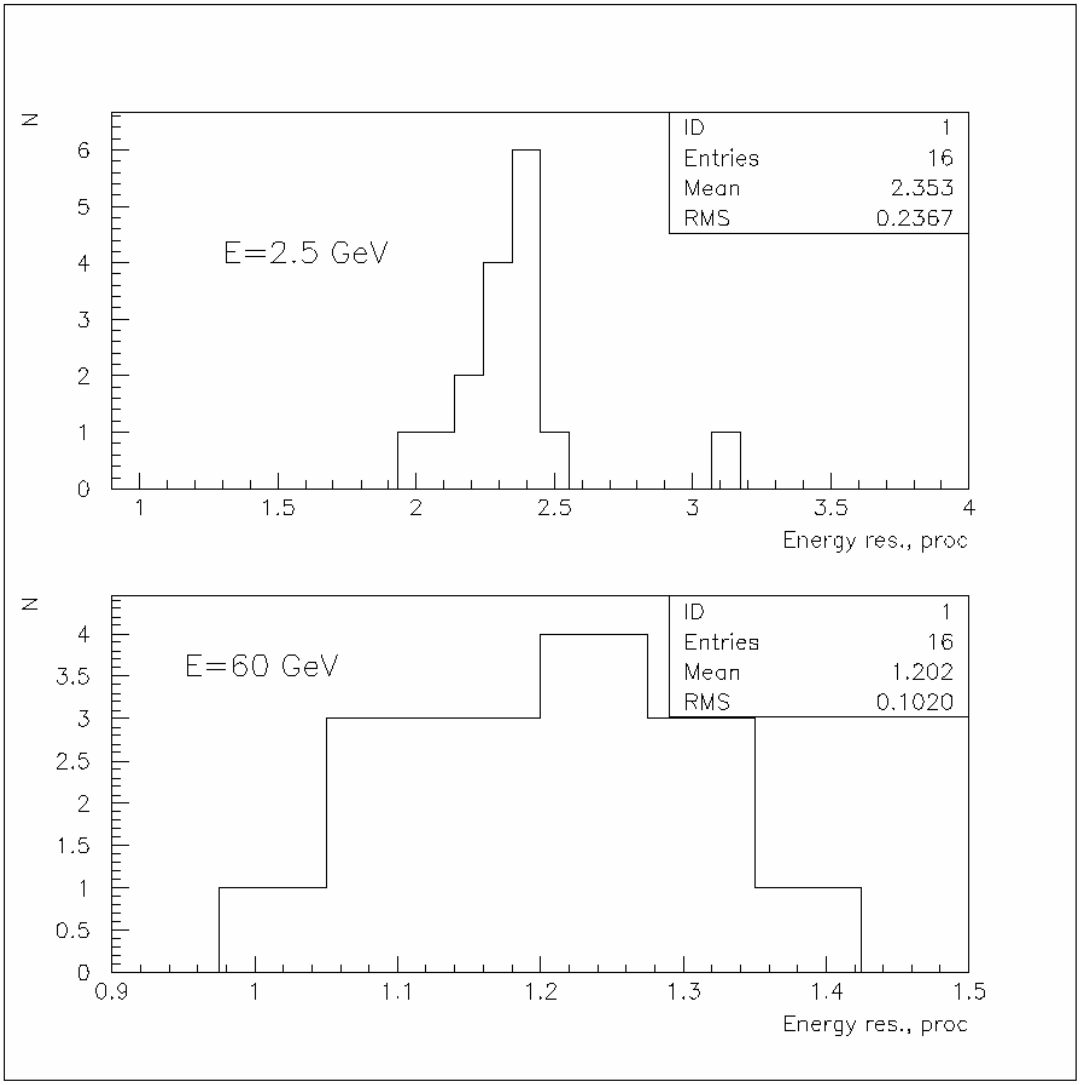
N
E=2.5 GeV
ID 1
Entries 16
Mean 2.353
RMS 0.2367
Energy res., proc
N
E=60 GeV
ID 1
Entries 16
Mean 1.202
RMS 0.1020
Energy res., proc

Fig. 15

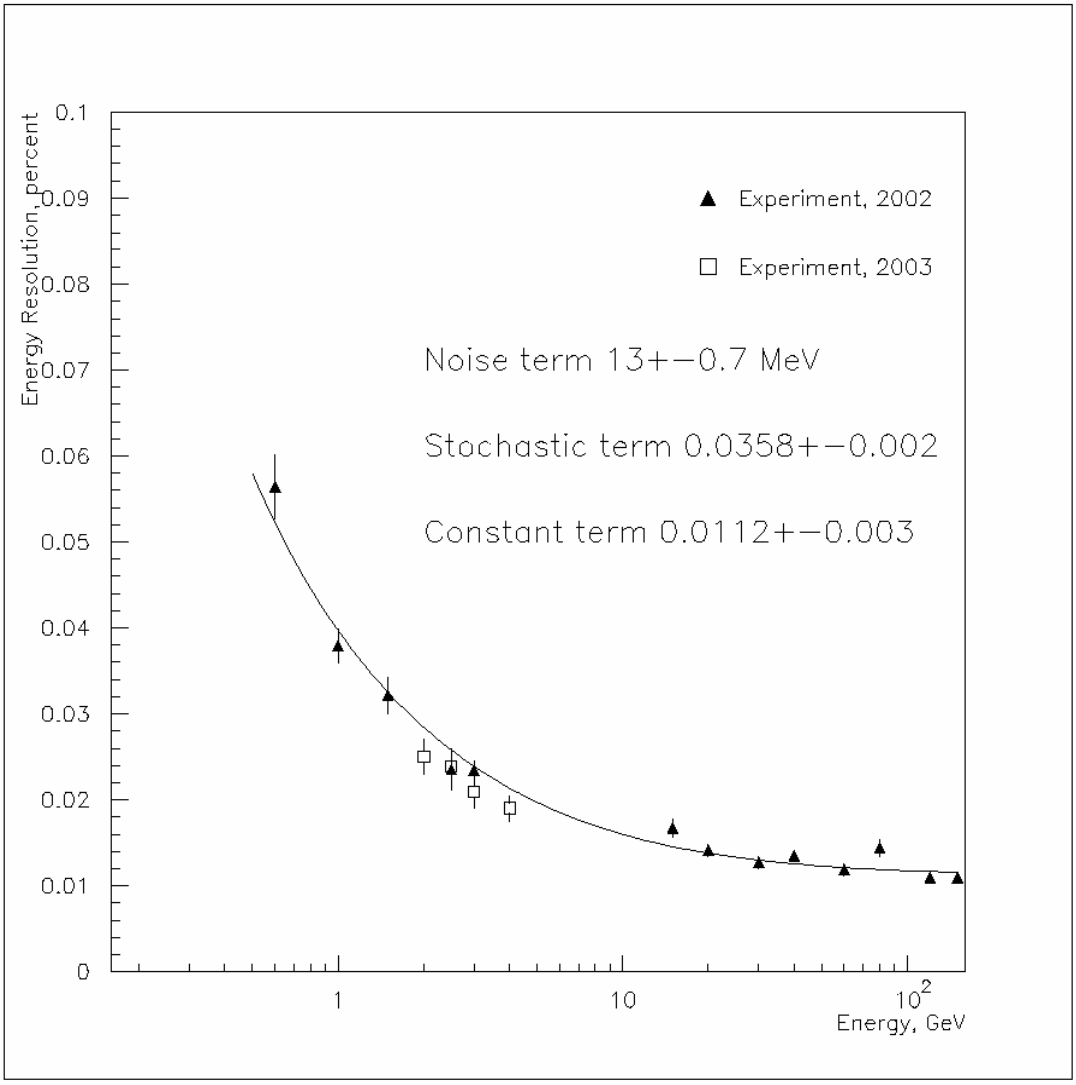
Energy Resolution, percent
0.1
0.09
0.08
0.07
0.06
0.05
0.04
0.03
0.02
0.01
0
1
10
10^2
Energy, GeV
Experiment, 2002
Experiment, 2003
Noise term 13+−0.7 MeV
Stochastic term 0.0358+−0.002
Constant term 0.0112+−0.003

Fig. 16

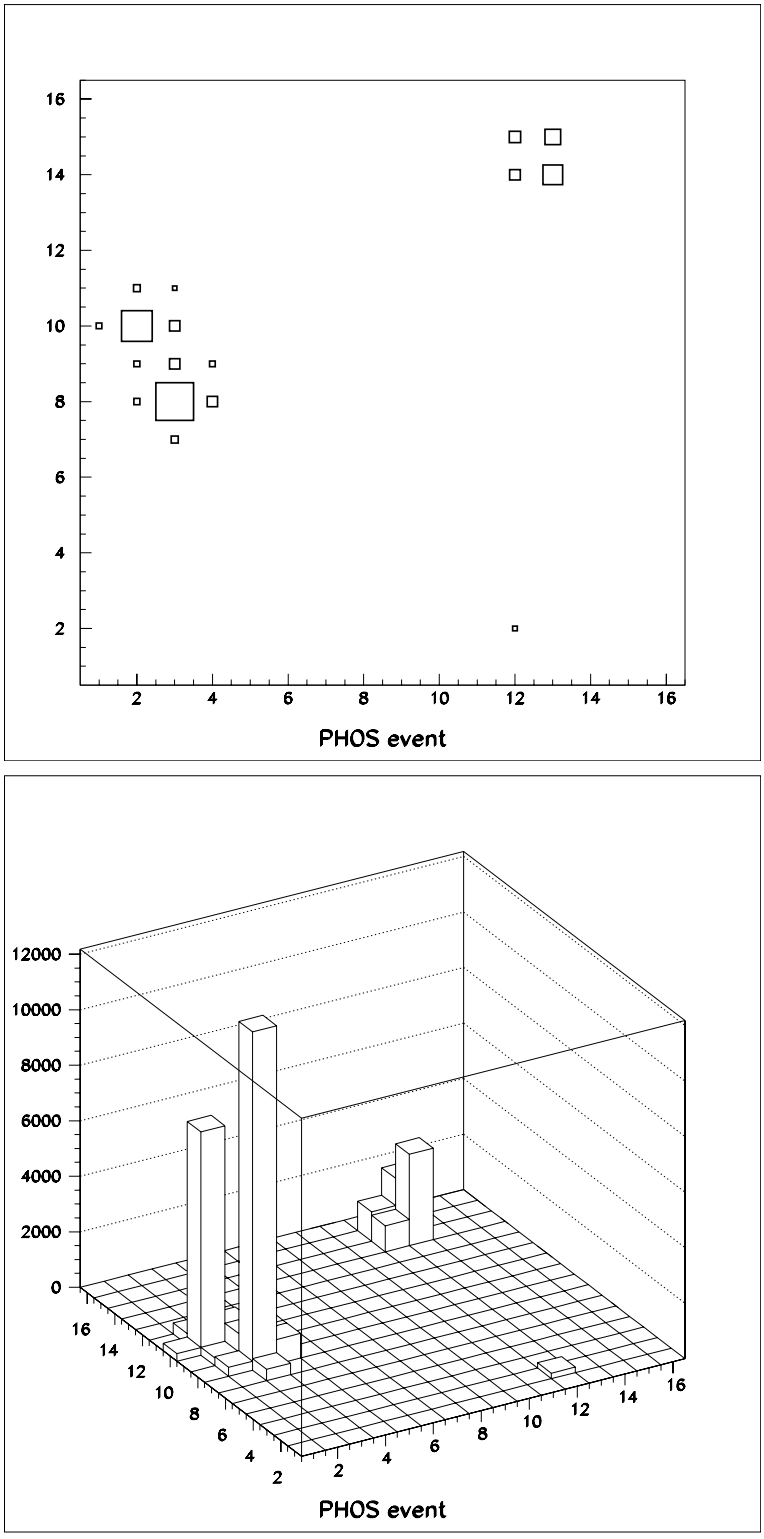
16
14
12
10
8
6
4
2
2
4
6
8
10
12
14
16
PHOS event
12000
10000
8000
6000
4000
2000
0
16
14
12
10
8
6
4
2
2
4
6
8
10
12
14
16
PHOS event

Fig. 17

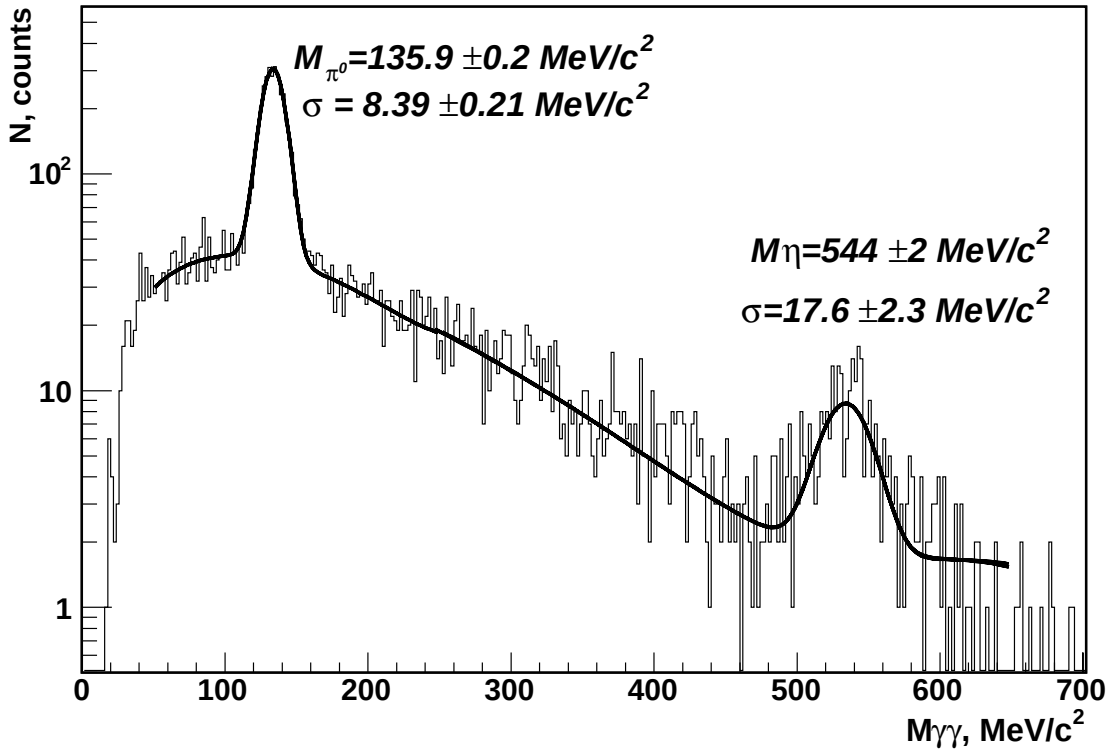
N, counts
10^2
10
1
M_{π^0}=135.9 ±0.2 MeV/c^2
σ = 8.39 ±0.21 MeV/c^2
Mη=544 ±2 MeV/c^2
σ=17.6 ±2.3 MeV/c^2
0
100
200
300
400
500
600
700
Mγγ, MeV/c^2

Fig. 18